# Synthesis and Characterisation of Nanoporous Folic Hemin Materials and Nanoporous Hemin Materials

**Adewale Olamoyesan[1,2,3]* and Chen Binghui[4]**

[1]*Department of Molecular Sciences, Faculty of Science and Engineering, Macquarie University, NSW, Australia*
[2]*Unversity of Lagos, Faculty of Science, Department of Chemistry, School of Foundation Studies, Akoka-Yaba, Lagos, Nigeria*
[3]*Wigwe University, College of Science and Computing, Isiokpo, Rivers, Nigeria*
[4]*Xiamen University, School of Energy and Chemical Engineering, Selangor, Malaysia*

## ABSTRACT

**Hemin like folic acid, FA, can replicate biological functions within inorganic materials. This study is aimed at fine-tuning the features of typical mesoporous silica derived using FA as a template referred to as nanoporous folic materials, NFM-1, by replacing FA progressively in the synthesis gels with equivalent moles of hemin to form nanoporous folic hemin materials, NFHM-1 (hemin, 3.12-50%), and nanoporous hemin materials, NHM-1. We found that increasing the ratio of hemin to FA decreases the intensity of the mesoscale peaks between 2θ (2-6°) and the stacking array of petrin of the folate that is gradually replaced by that of hemin. The spectroscopic features and XRD patterns for samples synthesised at 40°C were similar to those obtained at room temperature, RT. Various morphology such as spheres, twisted rods, hierarchical architectures, flower-like, and ribbons were observed for these samples.**

## KEYWORDS

**hemin, folic acid, nanoporous folic materials, nanoporous folic hemin materials, silica**

Received 28 December 2022, revised 25 December 2023, accepted 15 January 2024

## INTRODUCTION

Ever since the discovery of the mesoporous silica family of M41S in the very early '90s, arrays of these materials have been synthesised under acidic, alkaline, and neutral conditions using different types of surfactants or templates, terminal silica or organosilica sources, additives, and solvents at varying concentrations and, or temperatures. The essence of this drive is to improve these materials' features, impart functionality and extend their applications to other areas. These inorganic or organic–inorganic hybrid nanostructured materials have unique properties that make them versatile for different uses such as uniform and tunable porosity, and pore volume accessible to bulky reactants or chemicals.[1,2]

In recent times, supramolecular amphiphilic molecules have been explored as templates with the capability to replicate biological functions within inorganic materials. These important organic molecules self-assembly through a distinct form of hydrogen bonding between electron donating and accepting groups on the guanine or its analog into tetramers and these are later arranged into either columnar, cubic, or hexagonal mesophases, and with chiral structures.[3-5] The addition of costructure directing agents, CSDA, such as 3-aminopropyltriet-hoxysilane, APES, enables the template and silica ions to interact electrostatically, for which the protonated amino group of CSDA acts as charging matching ions. This synthesis route allows for the direct functionalisation of silica internal pore surface with aminopropyl groups, which are exposed by the removal of the template through a mild extraction process; thereby enhancing its adsorption and catalytic activities. NFM-1 made via this distinct self-assembly route was investigated for its release profile of the folate in the pores, and the calcined sample for carbon dioxide adsorption.[3,6] Noteworthy, the formation of these tetramers is possible at lower concentrations in water than that for micelles, as well these templates are cheap and eco-friendly as compared with the surfactants. Thus, an optimised stoichiometric molar ratio of 3:1 of APES to FA or guanosine monophosphate, GMP, was used to obtain fine-tuned silica with morphology of rods, gyroids, and spheroids.[4-6]

Folic acid is a vitamin B9, the synthetic form of naturally occurring folates (Figure 1a), an essential nutrient for the prevention of several disorders and being used as a target ligand in cancer cells.[7] Besides that folate and its derivatives are known to have optical and optoelectronic properties,[8,9] in that case, the direct introduction of hemin into the framework of NFM-1 as cotemplate could modify the optical activities as well as the morphology of these materials for photoluminescence, sensing, photodynamic and photothermal therapies, photocatalysis, asymmetric catalysis, and other applications.[10-13] Hemin, a metalloporphyrin with iron-nitrogen coordination at the macrocycle core and two carboxylate linkers, which are essential for bonding with metal ions and other positively charged moieties (Figure 1b). This compound is an important cofactor for enzymes and proteins such as cytochromes, hemoglobin, myoglobin, and peroxidases.[14-16]

In general, the optical and photocatalytic activities of mesoporous silica are enhanced by embedding a variety of metal oxides, dyes, porphyrins, and their derivatives in its pore cavities. Alternatively, these can be achieved through the self-assembly of porphyrins with covalently attached alkoxyl silyl groups during sol-gel reaction.[11-13,17-21] Through some forms of electrostatic interactions and careful molecular ordering of porphyrins and their hybrid nanostructures various sizes and morphology with unique properties for different applications were realised.[22,23] Xiaolan et al. encapsulated the functionalised hemin silylated precursor into a magnetite composite through a modified Stober method.[24] Likewise, Wei Yang et al. prepared silica nanoparticles doped with hemin in water/oil emulsion and the resulting material was employed to determine very low amounts of glucose.[25]

This report discusses how NFHM-1 and NHM-1 were prepared by introdicing hemin to replace equivalent moles of FA in NFM-1 synthesis protocol at RT and 40°C. We derive information on the self-assembly, interactions between ionic species, nucleation, and growth processes through in-situ conductivity measurements. In addition, the effect of hemin on the stacking of the folate, evidence of incorporation of hemin within the hybrids, optical properties, morphology and sizes of these asynthesised materials are determined by non-destructive

*To whom correspondence should be addressed
Email: adewale.olamoyesan@hdr.mq.edu.au; adewale.olamoyesan@gmail.com

ISSN 1996-840X Online / South African Chemical Institute / http://saci.co.za/journal

https://doi.org/10.17159/0379-4350/2024/v78a11

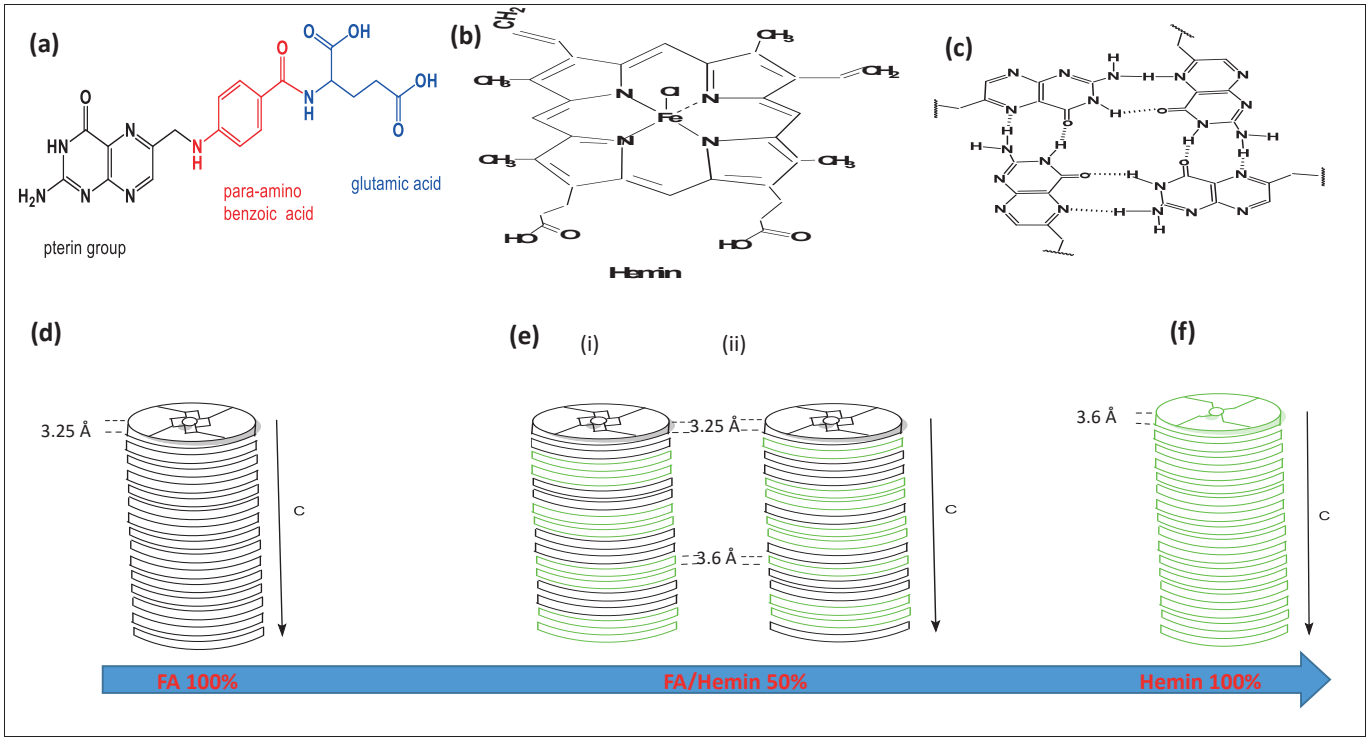


**Figure 1.** Structural formular of (a) FA and (b) hemin, (c) Hoogesten-type interactions between petrin groups (d) columnar stack of folate tetramers and e(i) orderly and (ii) randomly arranged stacks of folate tetramers and hemin H-aggregates of NFHM-1 (50%) synthesised with equivalent moles of both molecules as mixed templates in the synthesis gel, (f) stack of hemin aggregates. Black and green colour discs are representatives of folate tetramer disc and hemin aggregate, respectively

techniques. The intensity of low angle and folate stacking' peaks progressively decreases as the moles of hemin introduced to the synthesis gels increase to replace that of FA. All the samples with hemin exhibit characteristic Soret band and the Q bands which are weakly resolved as the mole of hemin in the template mixture decreases. Similarly, the emission spectra of these materials display a series bands in that the band at 604 nm decreases in intensity as FA decreases to hemin in the synthetic gels.

## EXPERIMENTAL

### Materials

The materials used for these syntheses are as follows hemin (98%), FA (99%), APES (99%), tetraethyl orthosilicate, TEOS (98%). These reagents were acquired from Sigma-Aldrich and used as received without being purified or altered.

### Conductivity/pH Measurements

Mettler Toledo SevenExcellence pH/mV conductivity meters equipped with a temperature sensor were used to collect the conductivity and pH measurements as a function of time, which were taken every 2 s along the whole process while continuously stirring the synthesis gels at desired temperatures.

### Powder XRD Analysis

Panalytical and Bruker diffractometers were used to collect the XRD patterns of the as-made materials with the same X-ray source (λ = 1.541Å) but different step size and time (of 0.044 and 56 s, 0.005 and 5 s respectively).

### Scanning Electron Microscopy

JEOL 7100 SEM was used to record the images of these samples. This particular type of SEM is equipped with a field emission gun and set to a low voltage of about 1 kV and at least a magnification of 250 X.

### Nitrogen adsorption/desorption isotherms

ASAP 2020 model of Micrometrics analyser was used for the measurement of the sorption isotherms of the calcined samples (NFM-1, NFHM-1 and NHM-1). These samples were degassed for 10 h at 120°C before the measurements were taken at 77K. Models used for the calculations of the surface area, total pore volume and the distribution of pore size are the same as stated in reference(3).

### Fourier Transform Infrared (FTIR) Spectroscopy

A model of spectrometer named iS50 from Thermo Scientific equipped with an ATR device, black diamond/ZnSe crystal and mercury cadmium telluride detector. All the spectra were collected in the range of 650-4000 $cm^{-1}$ and scanned for an average of 64 times to improve their signal-to-noise ratio.

### UV-vis Spectroscopy

JASCO V-760 UV-vis spectrophotometer was used to take the UV-vis spectra of the samples at RT. Each sample was dispersed in ethanol (0.12 mg/mL) and sonicated for 5 min before spectra measurement at a wavelength range of 200-700 nm, and the scan speed was set at 200 nm/min.

### Fluorescence Spectroscopy

JASCO fluorescence spectrometer was used to take the measurements at RT. The excitation wavelength of the sample solutions was set at 450 nm for hemin while the speed of scanning was set at 200 nm/min. Each sample was dispersed in ethanol (0.12 mg/mL) and sonicated for 5 min before spectra measurement.

### Synthesis of NFM-1

NFM-1 samples were prepared based on the procedure described by Atluri et al. with slight modifications.[3] The template solutions were first prepared by dissolving (0.847 g, 1.92 mmol) of FA in 60.48 mL of Mill-Q water under stirring for 1 h at 1000 rpm in closed containers at

RT and 40 °C, respectively. After the first 5 min of measurements of the media conductivity and pH, a mixture of APES (1.116 mL, 5.04 mmol) and TEOS (3.25 mL, 15.6 mmol) was added to each solution under constant stirring, and the measurements were continued for 20 min. Then the obtained reaction gels at RT and 40°C were left unstirred for 24 and 36 h respectively before treating hydrothermally for 24 h at 100 °C to improve the structural order and enhance the condensation of silica. The resultant synthesis gels were filtered and then rinsed with copious amounts of water and ethanol, and the obtained solids were allowed to dry overnight at RT. To extract the template from the pores of this mesoporous silica, 0.1 g of the as-synthesised solids were dissolved in 10 mL of ethanol/HCl (37%) mixture in a 90/10 weight % ratio, and this was refluxed for a day at 60 °C. After filtering and washing with water and ethanol, the resultant air-dried samples were heated in a furnace under air for 6 h at 550 °C.

### Synthesis of NFHM-1

These variants of NFM-1 were obtained by using FA and hemin as mixed templates. The amount of hemin introduced as cotemplate to replace equivalent moles of FA in the synthesis gels to give a series of NFHM-1 is illustrated in Table 1, and all other reaction parameters were kept constant as in NFM-1 synthesis.

### Synthesis of NHM-1

NHM-1 samples were synthesised using the same method as for the synthesis of NFM-1. To prepare the template solutions 1.252 g of hemin were dissolved in 60.48 mL of Milli-Q water, and all other reaction parameters were kept constant as NFM-1 synthesis.

## RESULTS AND DISCUSSION

Conductivity measures the ions in aqeous solutions which indicates their ability to conduct electricity. Typical conductivity of the early stages of formation of NFM-1 with and without hemin as cotemplate and NHM-1 at RT and 40 °C, respectively are shown in Figure 2(a and b). The template solutions were allowed to stabilise for 1 h, and conductivity was measured for 5 min before the addition of any other reagents. No change is observed in the conductivity curve (see Figure S1). FA is poorly soluble and hemin is insoluble in water, while the solubility of both is enhanced upon deprotonation of the carboxylic groups of these biomolecules by the addition of a mixture of APES (costructure directing agent, CSDA) and TEOS or an alkali solution to the template solutions.[3,4] Thus, the pH rapidly increased from 4.5 to 8.4 ca. and conductivity rose to its maximum, this suggests some ammonium species have formed that act as both catalysts for the hydrolysis step and charged matching ions to induce electrostatic interactions. Within the first few minutes the aqueous folate self-assembled into tetramers via hydrogen bonding by the pterin groups inside the core and the charged glutamic moieties are exposed to the exterior of it, where the *p*-amino benzoic acid groups are vital for the formation of columnar stacks of these tetramers stabilised through π-π interactions and through π-σ interactions to adopt chiral geometry along the c-axis.[3,4] On the same timescale with the formation of folate tetramers, the hemin aggregates were formed for the syntheses with it;[26,27] these aggregates could either be orderly or randomly arranged between the stacks of folate tetramers for syntheses with varying mole ratios of hemin to FA as mixed templates (Figure 1a-f). Following that the oppositely charged ions of CSDA, and carboxylate moieties of folate stacks and, or hemin aggregates attracted to themselves, as the alkoxyl groups of both silica sources hydrolysed to give silanol groups (≡SiOH) and eventually through condensation these reacted to form siloxane bonds (≡Si–O–Si≡) and water or ethanol as a by-product (Scheme 1).

For NFM-1, a monotonic decrease in the conductivity curve was observed after maximum conductivity was reached, but a gradual decline in the conductivity was seen for the sample with 3.125% hemin, which became more rapid with the increase in concentrations of hemin. This noticeable decline in conductivity over time is as result

**Table 1.** NFHM-1 samples with varying amounts of hemin to FA in the synthesis gel at both RT and 40 °C.

| Sample Name | FA (g) | Hemin (g) | $H_2O$ (g) | APES (mL) | TEOS (mL) |
|---|---|---|---|---|---|
| NFHM-1 (hemin, 3.125%) | 0.821 | 0.039 | 60.48 | 1.12 | 3.25 |
| NFHM-1 (hemin, 6.25%) | 0.795 | 0.078 | 60.48 | 1.12 | 3.25 |
| NFHM-1 (hemin, 12.50%) | 0.746 | 0.156 | 60.48 | 1.12 | 3.25 |
| NFHM-1 (hemin, 25%) | 0.636 | 0.313 | 60.48 | 1.12 | 3.25 |
| NFHM-1 (hemin, 50%) | 0.424 | 0.626 | 60.48 | 1.12 | 3.25 |

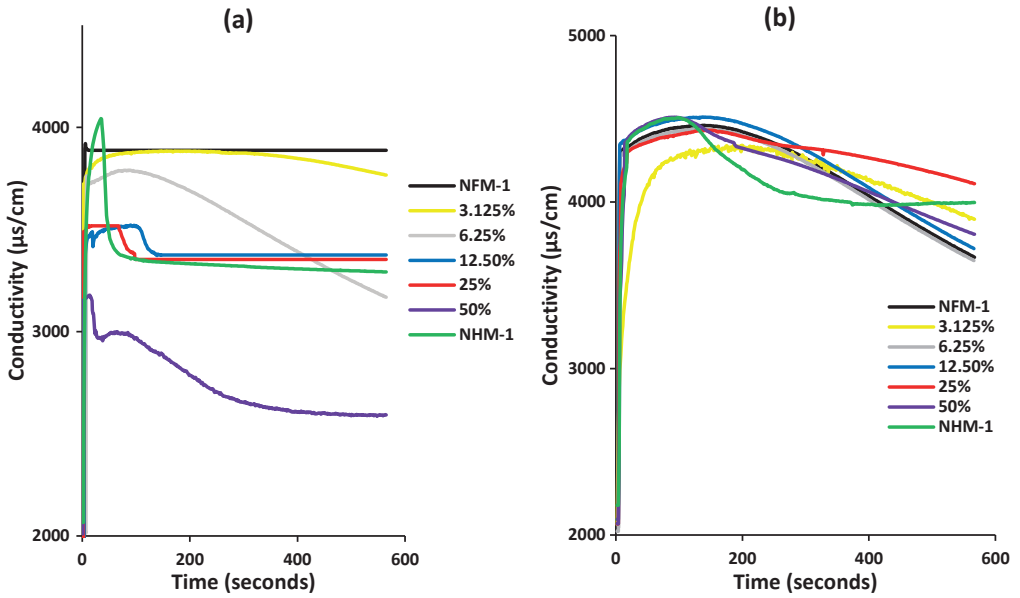


**Figure 2.** Conductance curves of the early stages of formation of NFM-1, NFHM-1 (hemin, 3.125-50%) and NHM-1 synthesised at (a) RT and (b) 40°C.

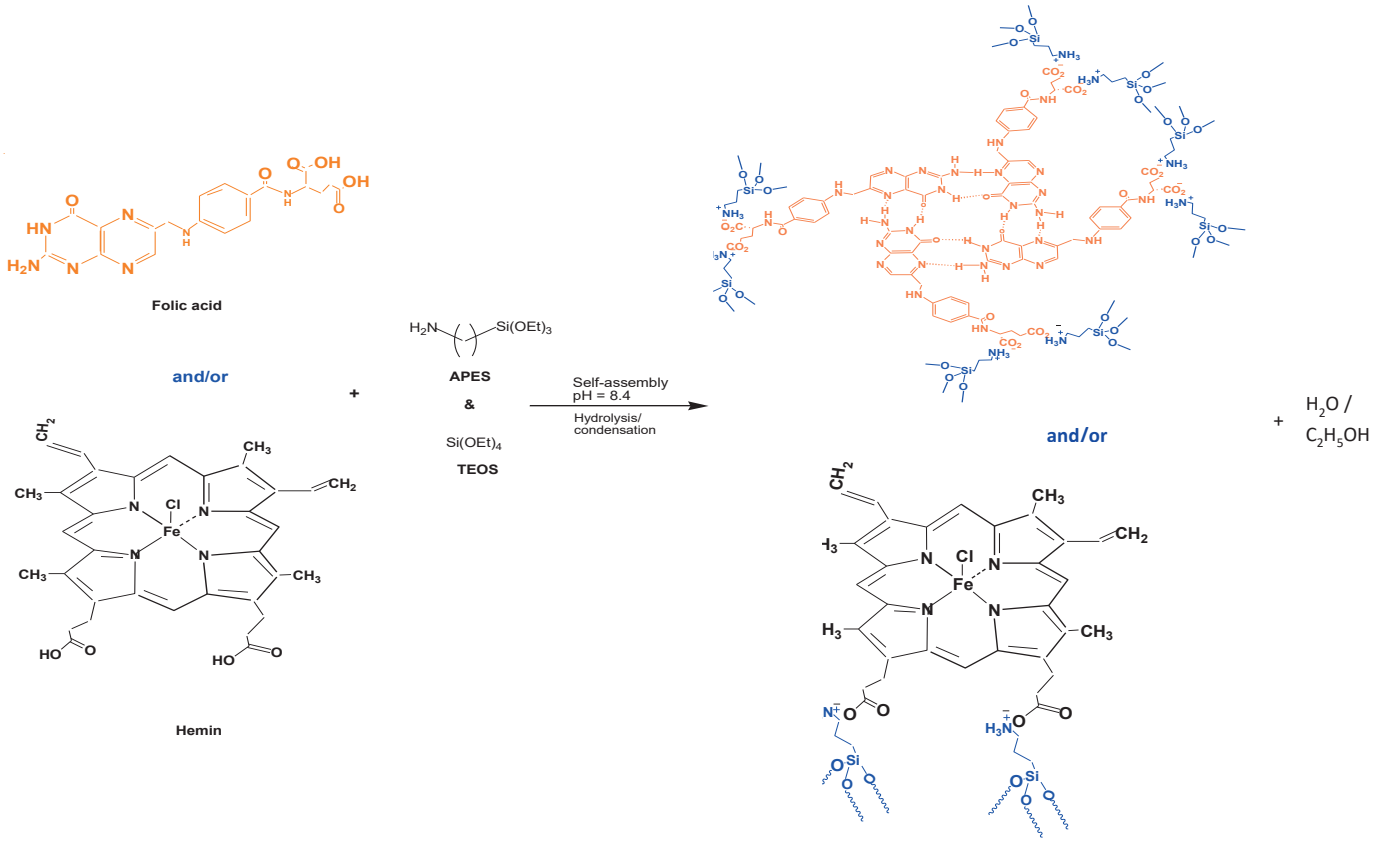


**Scheme 1.** Schematic representation of the self-assembly, electrostatic interactions between the deprotonated folate tetramers, and,or hemin aggregates with protonated ammonium species derived from CSDA, hydrolysis and condensation reactions of silica precursors to give organic-inorganic hybrid materials

of the consumption of charged species accompanied by condensation of hydrolysate species that give rise to silica/template mesophases. An obvious discontinuity can be seen between 38 and 130 s for syntheses with (6.25-100%) hemin, while that for the other systems appeared at a higher time range due to slower hydrolysis (Figure 2a). After the initial stage of synthesis, the samples were left unstirred to age for a day. As aging time significantly affects the properties of mesoporous silica, this allows for the continuation of the growth process over time until homogeneous or uniform particle sizes are attained.[28] The maximum conductivity was higher for samples synthesised at 40 °C than that at RT, as is typical for electrolytes. These samples' discontinuity was observed at a higher timescale, which implies slower hydrolysis as compared with syntheses at RT, and expectedly condensation rate is faster (Figure 2b). It was observed that the rate of hydrolysis increases as the amount of hemin increases in the reaction mixtures. Hence, the sample with hemin on its own as a template displayed discontinuity at 258 s and the others appeared at a slightly higher time range.

To determine the ordering of the mesophases XRD analysis was performed on them. According to Figure 3, the diffractograms for NFHM-1 (hemin, 3.125-50%) and NHM-1 in comparison to that of typical NFM-1 sample synthesised at RT show two well-resolved peaks at low angle that can be indexed as (10) and (11) reflections in the 2-dimensional hexagonal unit cell respectively with a unit cell parameter between 4.1-5 nm, and a peak at 2θ 22° corresponding to the amorphous silica wall for all the samples. The existence of the two peaks at the low angle region is indicative of the formation of long-range ordered mesoporous silica. Intensities of these two peaks at low angle diminish progressively as the amounts of hemin in the synthesis mixtures increases, as well as the π-π stacking for folate tetramers with a d-spacing of 0.325 nm as the corresponding stacking peak of macrocycle core of hemin gradually began to appear at 2θ 24.33° with a d-spacing of 0.36 nm. Accompanying the appearance of the hemin stacking peak are the peaks with d-spacing of 1.30, 0.769, 0.664, and 0.538 nm as observed in the X-ray diffractogram of hemin (see Figure S2), which are most intense for NFHM-1 (hemin, 50%) and NHM-1. These peaks with their coresponding stacking peak indicate the incorporation of hemin into the inorganic-organic composites with either hemin on its own or as mixed template systems of FA/hemin in varying ratios. Hemin like most porphyrins may overlap in a face-to-face style known as H-aggregates or otherwise, presumably, these aggregates could be randomly or orderly arranged between the stacks of folate tetramers for NFHM-1 (hemin, 3.125-50%) samples (Figure 1e (i) and (ii)). The peak with the d-spacing of 1.30 nm can be ascribed to (001) refraction of hemin layers that appeared only in samples with hemin, that at 2θ 22° corresponding to the amorphous silica wall was observed for all the samples. In comparison with the samples prepared at 40°C, the stacking peaks for both folate and hemin are more intense, while the peaks at the low-angle are less intense for products obtained at RT, which implies less long-range hexagonal packing.

Figure 4 presents the FT-IR spectra of as-synthesised NFM-1 and NFHM-1 with varying ratios of hemin to FA (as mixed templates) and NHM-1. The fingerprint for C=O stretching vibration appeared at 1700 $cm^{-1}$, which was weak for all the silica with folate, mixtures of folate and hemin, and wholly hemin compared to hemin and FA. The weak intensity for all the silica is indicative of CSDA electrostatically interacting with carboxylate ions in both the FA and hemin (see also Figure S3), which is evidence that these hybrids are formed via the ($S^-M^+I^-$) mechanism.[29] Infrared fingerprints that are characteristics of the presence of aromatic rings or alkene and the protoporphyrin (IX) ring are the stretching vibrations of C=C and C=N at 1604 $cm^{-1}$ and 1500 $cm^{-1}$ respectively, and the latter confirmed the existence of an aromatic ring. Moreover, the peak at 1393 $cm^{-1}$ is ascribed to the symmetric bending of C-H in $CH_3$ of hemin, which was stronger for NFM-1, NFHM-1, and NHM-1 samples than hemin due to the ordered assembly of silica-template(s). The bands which are typical for silicate materials are found at 3350,1645 1050, 766, and 945 $cm^{-1}$ and are assigned to stretching vibrations of O-H and absorbed water, symmetric and asymmetric stretching vibrations of siloxane group

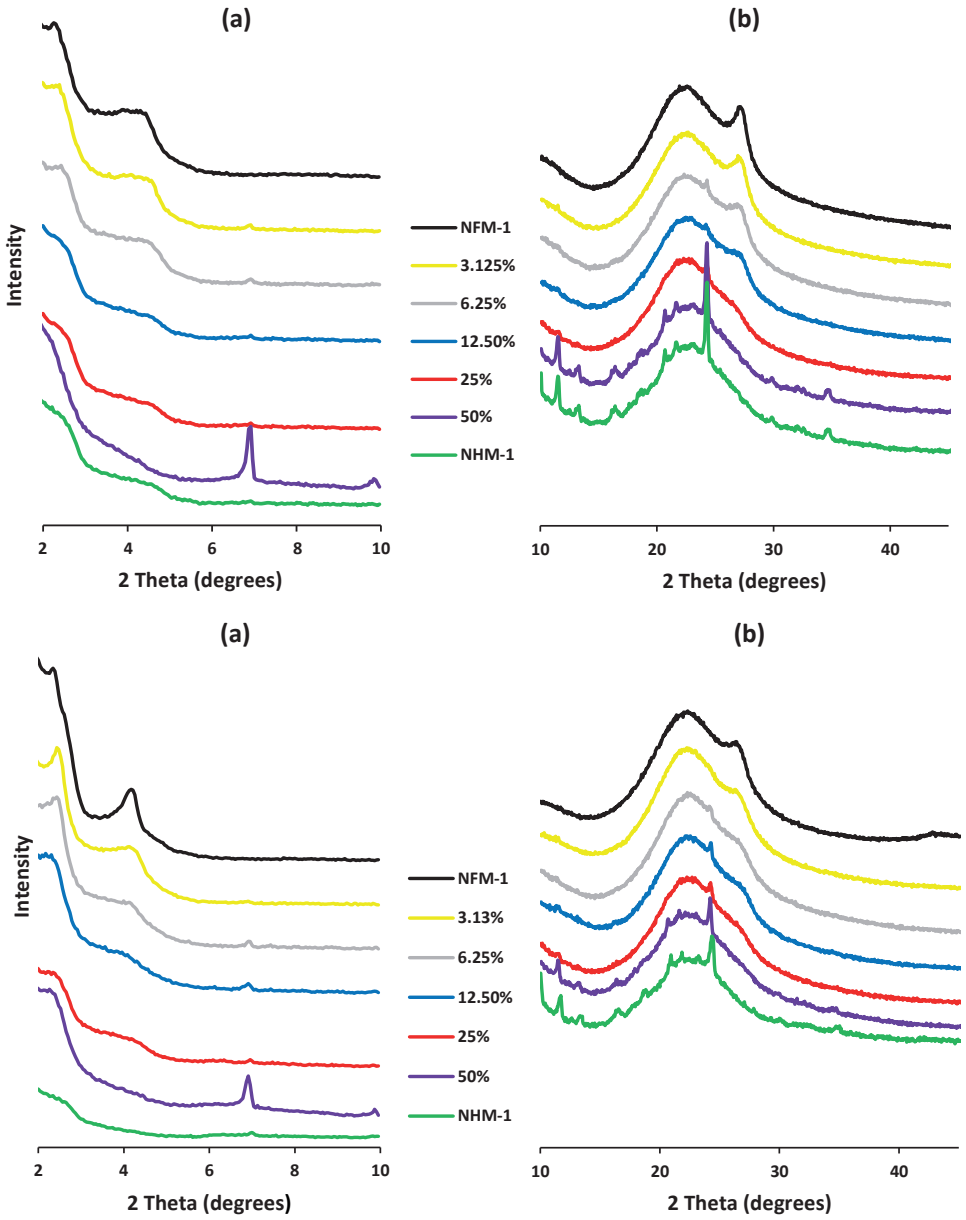


**Figure 3.** Powder XRD diffractograms of as-made samples of NFM-1, NFHM-1 (hemin, 3.125-50%) and NHM-1 synthesised at RT (above) and at 40°C (below) recorded at (a) low and (b) high angles.

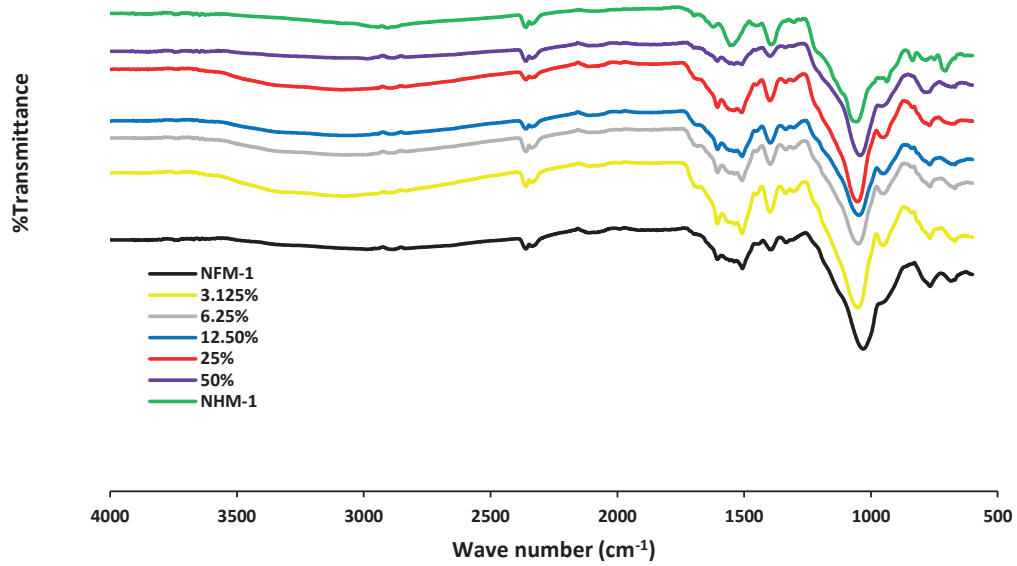


**Figure 4.** FT-IR spectra of as-synthesised NFM-1, NFHM-1 (hemin, 3.125-50%) aand the sample with absolute hemin as template, NHM-1 prepared at RT.

in the silica framework, and bond stretching of Si–OH, respectively. Also, the bands for N–H stretching and bending at 3400 $cm^{-1}$ and 1640 $cm^{-1}$ respectively overlapped with that of O–H at both wave numbers. The hemin existence in the hybrids can be proved by the presence of iron (Fe) contrary to FA. Therefore, elemental composition analysis of NFHM-1 and NHM-1 obtained by EDXS revealed these nanostructures consist of Fe and Cl besides Si, O, N, and C as in NFM-1. This provides evidence of hemin presence within the mesopores (see Figure S4).

Textural information of these samples was obtained from sorption isotherms (see Figure 5a and b). The isotherms in Figure 5a are true to form as with materials with mesopores,[30] have monolayer-multilayer adsorption at relatively low pressure ($p/p^o$ 0.05-0.2), with a rare hysteresis loop within 0.45 to 1[31,32] that accompanied capillary condensation. This loop indicates the dissimilarity between the adsorbed and the desorbed $N_2$, of which size gradually increases for samples with 12.5-50% hemin to FA. However, all the samples with less than 12.5% hemin and absolute hemin except for NFM-1 have the least hysteresis loop size of approximately 1 $cm^3/g$, STP (standard temperature and pressure). This particular type of hysteresis loop might show some defects in the hexagonal channel matrix of this mesoporous silica.[33] Figure 5(b) illustrates the distribution curves of the pore size centred around 3.09, 2.45, and 2.31 nm for samples synthesised with fractions of hemin < 12.5%. On the other hand, the other samples displayed primary mesopore centred at about 16.7 nm, accompanied by secondary mesopores, in addition, samples with 25 and 100% hemin possessed micropores at about 1.55 nm in the same range as that with 6.125% hemin. The incremental pore volume for mesopores between 8.2-17 nm increases for NFHM-1 (hemin, 12-100%) as the concentration of hemin increases in the synthesis gels.

Table 2 illustrates that the surface area and pore volume of typical NFM-1 declines as the hemin increases in the synthesis gels. NHM-1 has the least surface area appreciably less than 100 $m^2/g$ and its pore volume is approximately one-half of that estimated for NFM-1, while the other hybrids with hemin in the framework have the surface area and pore volume within 337-170 $m^2/g$ and 0.2-0.089 $cm^3/g$ respectively.

How these samples respond to ultraviolet light was examined with complementary spectroscopies as can be seen in Figure 6 (a and b). UV-vis spectrum of free hemin exhibited an intense Soret band at 400 nm and two weak Q bands at 500 and 636 nm, respectively. The organic-inorganic hybrids obtained with hemin in entirety and as cotemplate with FA showed characteristic Soret band (at 400 nm) suggestive of the formation of hemin aggregates,[26,27] and the band at 247 nm ascribed to Si-O-Si and the two Q bands were not discernible for samples with less than 25% hemin to FA. The latter Q band at 636 nm was slightly blue-shifted by approximately 2 nm for the hybrids with hemin, indicating the formation of H-aggregates. NFM-1 sample exhibited a broad band at a lower wavelength for siloxane and the corresponding FA absorption bands at 291 and 367 nm (see Figure S5(a and b)). These were weakly resolved for all the samples with FA. The fluorescence spectra of these samples excited at 450 nm showed a series of nearly the same bands at 483, 520, 530 and 676 nm, as well as a broad band at about 602 nm whose intensity dropped by an average of 39.35% as hemin is introduced incrementally to replace equivalent moles of FA in the synthesis gel in comparison with free hemin (Figure 6b). Both UV and fluorescence spectra for samples synthesised at 40°C were similar to those obtained at RT (figures not shown).

The morphology and size of the as-synthesised samples were determined by SEM using low voltage dosage at about 0.8-1 kV to reduce the charging effect due to the insulating properties of most porous crystals, as this usually improves the image resolution (otherwise

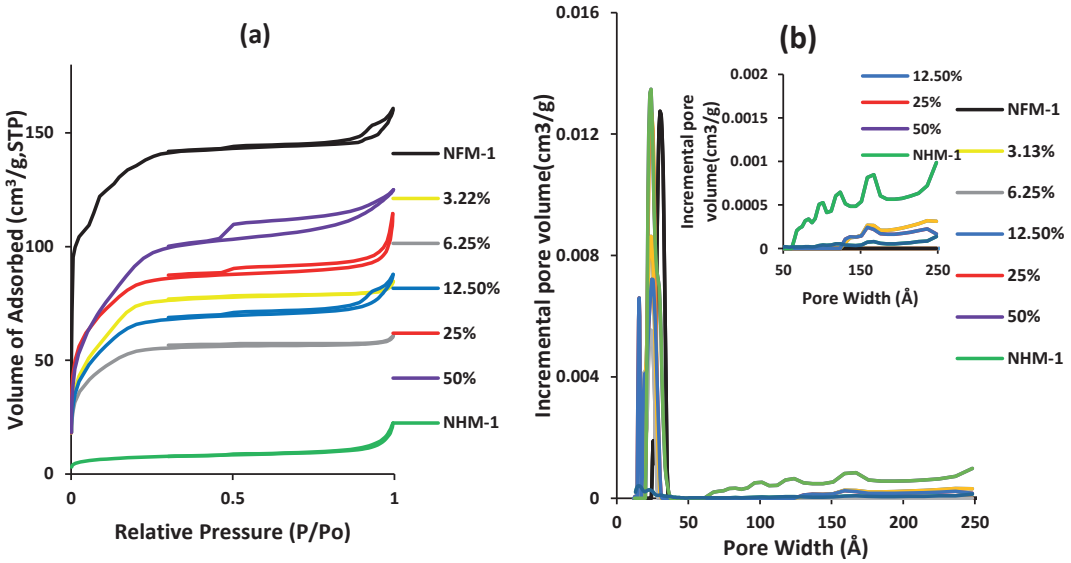


**Figure 5.** The nitrogen adsorption-desorption isotherms and pore distribution curves for calcined samples of NFHM-1 (hemin, <100%) and NHM-1 synthesised at RT.

**Table 2.** Textural properties of calcined NFM-1, NFHM-1 (hemin <100%) and NHM-1 samples synthesised at RT.

| Sample | $S_{BET\ (m^2/g)}$ | $V_p$ ($cm^3/g$) | Dp (nm) | $D_{XRD}$ (nm) | $A_0$ (nm) |
|---|---|---|---|---|---|
| NFM-1 | 794 | 0.400 | 3.031 | 3.428 | 4.428 |
| NFHM-1 (hemin, 3.125%) | 254 | 0.140 | 2.452 | 3.189 | 4.189 |
| NFHM-1 (hemin, 6.25%) | 179 | 0.089 | 1.594,2.010,2.309 | 3.117 | 4.117 |
| NFHM-1 (hemin, 12.5%) | 222 | 0.125 | 2.300,..,12.30,16.70 | 3.117 | 4.117 |
| NFHM-1 (hemin, 25%) | 273 | 0.137 | 1.583,2.524,..,16.70 | 3.328 | 4.328 |
| NFHM-1 (hemin, 50%) | 327 | 0.206 | 2.308,…,16.70 | 3.823 | 4.823 |
| NHM-1 | 25 | 0.017 | 1.523,2.381,…,16.70 | 3.612 | 4.612 |

$S_{BET}$, BET surface area; $V_p$, specific pore volume; $D_p$, Pore diameter from average pore diameter; $D_{XRD}$, pore diameter estimated using d-spacing value form XRD assuming a pore wall thickness of 1.0 nm ($a_o$-1nm); $a_o$ = unit cell dimension ($a_o = 2d_{100}/sqr\ (3)$).

known as gentle beam mode). The SEM images of the NFM-1 sample synthesised at RT showed the morphology of sphere and rod particles in quantitative amounts of 65:35% based on a 100-particle count; the diameter and length of the rods varied approximately from 0.4-0.6 μm and 7-13 μm respectively, while the diameter of spheres averaged 2 μm (Figures 7a-d and S6). Variants of this pristine silica obtained by introducing hemin in sequential order to replace equivalent moles of FA in the synthesis gels were mainly spherical particles. It was

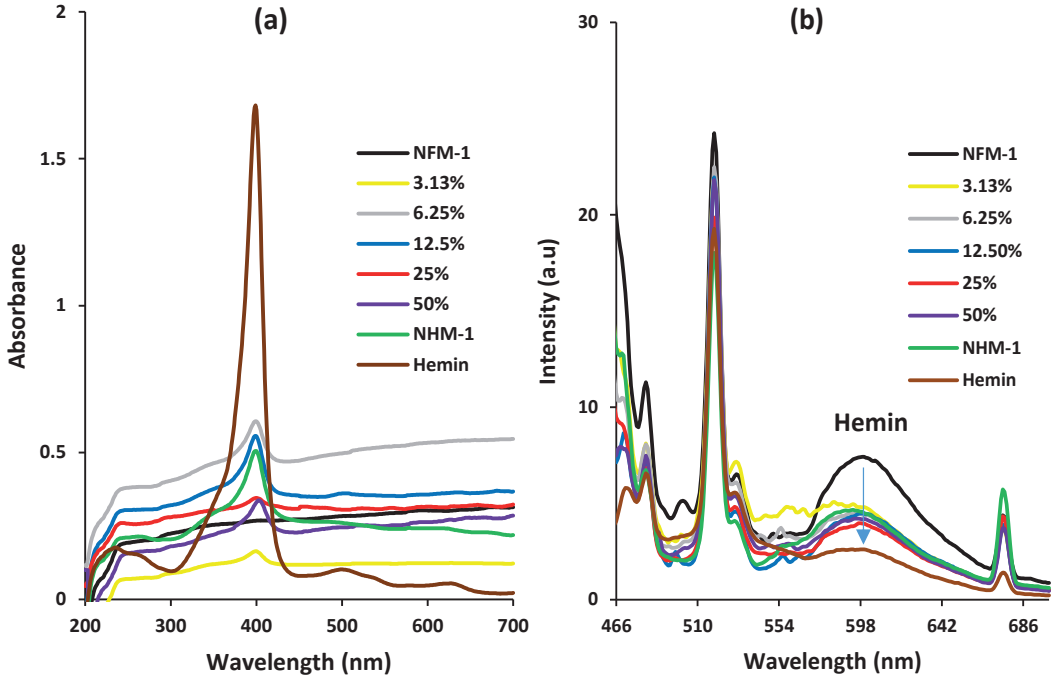


**Figure 6.** UV-vis absorption (a) and fluorescence spectra (b) of NFM-1, its variants with hemin as cotemplate with FA, NHM-1 and free hemin dispersed in ethanol.

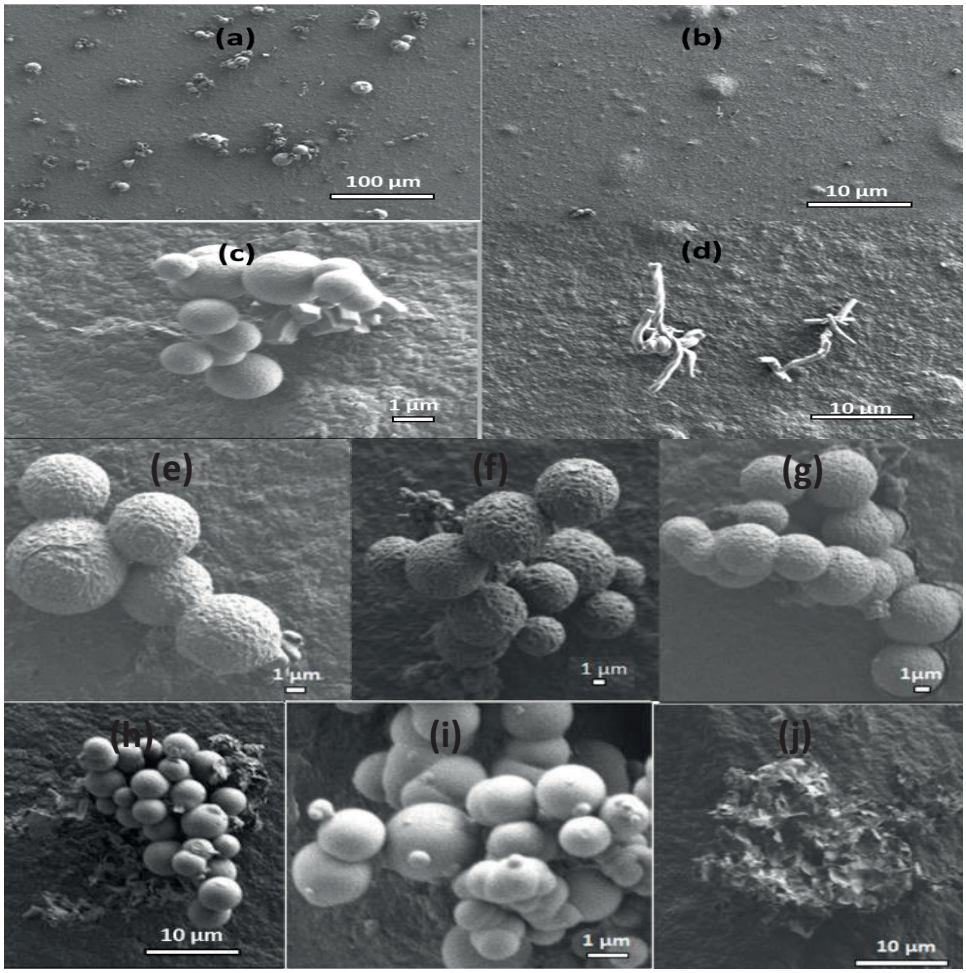


**Figure 7.** Scanning electron micrographs of samples of NFM-1 without and with hemin as cotemplate with increasing amount of hemin to FA namely: (a-d) NFM-1; (e) NFHM-1 (hemin, 3.125%); (f) NFHM-1 (6.25%); (g) NFHM-1 (hemin, 12.5%); (h) NFHM-1 (hemin, 25%); (i) NFHM-1 (hemin, 50%); (j) NHM-1 synthesised at RT.

observed that as the percentage of hemin in the synthesis gel increases from 3.125-12.5% these particles' average diameter increases from 4-5.5 µm, however, the average diameter decreases from 3.6-1.8 µm as hemin increases from 25-50%. A flower-like morphology is displayed by the sample with absolute hemin, NHM-1, and a mixture of this and sphere was observed in the sample synthesised with 25% hemin as mixed templates (Figure 7e-j). For the NFM-1 sample synthesised at 40°C rod particles of approximately 0.5 µm in diameter, which are mostly aggregated were observed (Figure S7). With the incremental introduction of hemin into the synthesis gels, hierarchical morphology of fibres, spheres, radial rods, and faceted spheres was seen except for NFHM-1 (hemin, 12.5%), NFHM-1 (hemin, 50%) and NHM-1 which displayed predominately irregular shape particles, spheres and folded ribbons respectively (Figure 8a-h).

## CONCLUDING REMARKS

FA and hemin, are important biomolecules for the prevention of several diseases, and cofactors of enzymes and proteins respectively, with distinct optical properties. These were employed singly and as mixed templates to synthesise novel mesoporous silica. We found that synthesis temperature and the mole of hemin to FA are important factors that induce morphological and dimension changes for these nanoparticles. A series of morphology including spheres, rods, fibres, faceted spheres, flower-like, and folded ribbons were observed. In addition, the features of the pristine NFM-1 were tuned as the hemin was introduced sequentially into the synthesis gel to replace equivalent moles of FA. Hemin, being a metalloenzyme with peroxidase activity, may inspire the applications of these new nanoporous materials as catalysts and biosensors. Future work should therefore include follow-up work on their utilisation as peroxidase catalysts for the oxidation of glucose and other substrates and as photocatalysts for the degradation of industrial textile wastes.

## ACKNOWLEDGEMENTS

Adewale Olamoyesan would like to thank Russell Field for training and granting him access to use the new X-ray diffractometer, as this saves me the trouble of commuting to the University of Technology Sydney for XRD analysis. Olamoyesan is extremely grateful to the provider of the fund for this research.

## SUPPLEMENTARY MATERIAL

Supplementary figures and tables referred to in this article are available online.

## ORCID IDS

Adewale Olamoyesan: https://orcid.org/ 0000-0002-9879-6726
Chen Binghui: https://orcid.org/0000-0001-7207-7486

## REFERENCES

1. ALOthman Z, ALOthman ZA. A review: fundamental aspects of silicate mesoporous materials. Materials (Basel). 2012;5(12):2874–2902. https://doi.org/10.3390/ma5122874.
2. Asefa T, Tao Z. Mesoporous silica and organosilica materials—review of their synthesis and organic functionalization. Can J Chem. 2012;90(12):1015–1031. https://doi.org/10.1139/v2012-094.
3. Atluri R, Iqbal MN, Bacsik Z, Hedin N, Villaescusa LA, Garcia-Bennett AE. Self-assembly mechanism of folate-templated mesoporous silica. Langmuir. 2013;29(38):12003–12012. https://doi.org/10.1021/la401532j.
4. Atluri R, Hedin N, Garcia-Bennett AE. Nonsurfactant supramolecular synthesis of ordered mesoporous silica. J Am Chem Soc. 2009;131(9):3189–3191. https://doi.org/10.1021/ja8096477.
5. Bueno-Alejo CJ, Villaescusa LA, Garcia-Bennett AE. Supramolecular transcription of guanosine monophosphate into mesostructured silica. Angew Chem Int Ed. 2014;53(45):12106–12110. https://doi.org/10.1002/anie.201407005.
6. Zhou C, Garcia-Bennett AE. Release of folic acid in mesoporous NFM-1 silica. J Nanosci Nanotechnol. 2010;10(11):7398–7401. https://doi.org/10.1166/jnn.2010.2823.
7. Hilgenbrink AR, Low PS. Folate receptor-mediated drug targeting: from therapeutics to diagnostics. J Pharm Sci. 2005;94(10):2135–2146. https://doi.org/10.1002/jps.20457.
8. Mitchell HK. Folic acid. IV. Absorption spectra. J Am Chem Soc. 1944;66(2):274–278. https://doi.org/10.1021/ja01230a035.

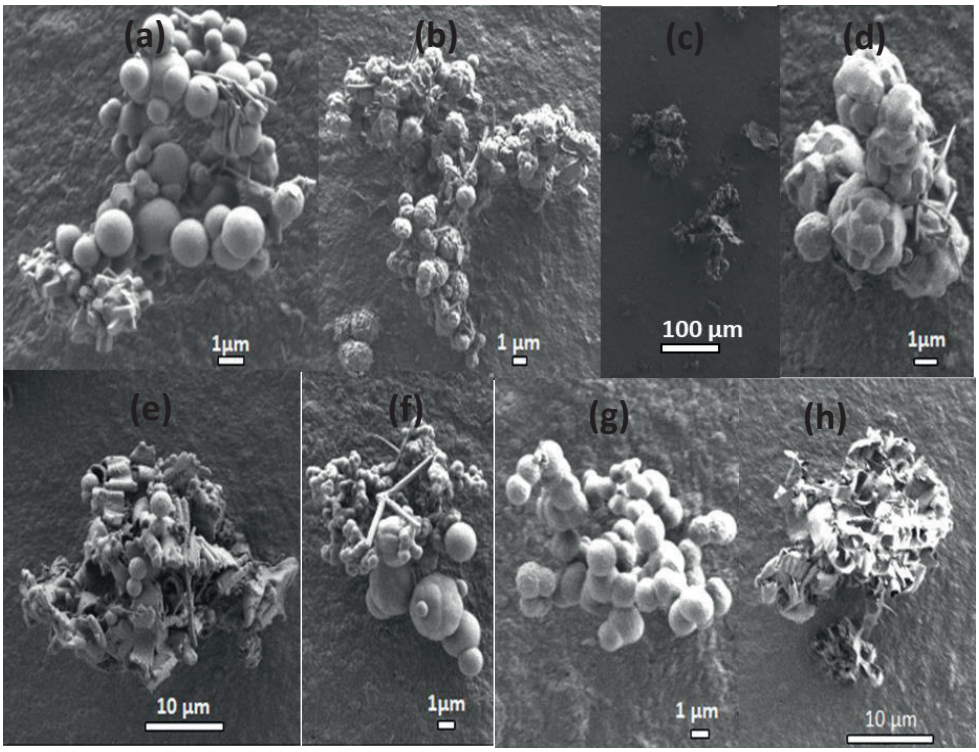


**Figure 8.** Scanning electron micrograms of samples of NFM-1 with hemin as cotemplate with increasing amount of hemin to folic acid namely: (a) NFHM-1 (hemin, 3.125%); (b) NFHM-1 (hemin, 6.25%); (c) NFHM-1 (hemin, 12.5%); (d-f) NFHM-1 (hemin, 25%); (g) NFHM-1 (hemin, 50%); (h) NHM-1 synthesised at 40°C.

9. Tyagi A, Penzkofer A. Fluorescence spectroscopic behaviour of folic acid. Chem Phys. 2010;367(2-3):83–92. https://doi.org/10.1016/j.chemphys.2009.10.026.
10. Ishihara S, Labuta J, Van Rossom W, Ishikawa D, Minami K, Hill JP, Ariga K. Porphyrin-based sensor nanoarchitectonics in diverse physical detection modes. Phys Chem Chem Phys. 2014;16(21):9713–9746. https://doi.org/10.1039/c3cp55431g.
11. Wang H, Song Y, Wang Z, Medforth CJ, Miller JE, Evans L, Li P, Shelnutt JA. Silica– Metal Core– Shells and Metal Shells Synthesised by Porphyrin-Assisted Photocatalysis. Chem Mater. 2008;20(24):7434–7439. https://doi.org/10.1021/cm802143d.
12. Wang J, Zhong Y, Wang X, Yang W, Bai F, Zhang B, Alarid L, Bian K, Fan H. pH-Dependent Assembly of Porphyrin–Silica Nanocomposites and Their Application in Targeted Photodynamic Therapy. Nano Lett. 2017;17(11):6916–6921. https://doi.org/10.1021/acs.nanolett.7b03310.
13. Magaraggia M, Jori G, Soncin M, Schofield CL, Russell DA. Porphyrin–silica microparticle conjugates as an efficient tool for the photosensitised disinfection of water contaminated by bacterial pathogens. Photochem Photobiol Sci. 2013;12(12):2170–2176. https://doi.org/10.1039/c3pp50282a.
14. Zhang G, Dasgupta PK. Hematin as a peroxidase substitute in hydrogen peroxide determinations. Anal Chem. 1992;64(5):517–522. https://doi.org/10.1021/ac00029a013.
15. Meunier B, De Visser SP, Shaik S. Mechanism of oxidation reactions catalyzed by cytochrome P450 enzymes. Chem Rev. 2004;104(9):3947–3980. https://doi.org/10.1021/cr020443g.
16. Shaik S, Cohen S, Wang Y, Chen H, Kumar D, Thiel W. P450 Enzymes: Their Structure, Reactivity, and Selectivity- Modeled by QM/MM Calculations. Chem Rev. 2010;110(2):949–1017. https://doi.org/10.1021/cr900121s.
17. Chandra D, Yokoi T, Tatsumi T, Bhaumik A. Highly Luminescent Organic–Inorganic Hybrid Mesoporous Silicas Containing Tunable Chemosensor inside the Pore Wall. Chem Mater. 2007;19(22):5347–5354. https://doi.org/10.1021/cm701918t.
18. Li L-L, Fu X-F, Ren Z, Zhao Y-G, Feng W, Yan C-H. Hierarchical Self-Assembly of Superlattice Hybrids Consisting of Periodic and Alternating Cores of Porphyrin Molecules Separated by Nanoscale Silica Walls. Langmuir. 2010;26(20):15730–15733. https://doi.org/10.1021/la1034036.
19. Osica I, Imamura G, Shiba K, Ji Q, Shrestha LK, Hill JP, Kurzydlowski KJ, Yoshikawa G, Ariga K. Highly Networked Capsular Silica–Porphyrin Hybrid Nanostructures as Efficient Materials for Acetone Vapor Sensing. ACS Appl Mater Interfaces. 2017;9(11):9945–9954. https://doi.org/10.1021/acsami.6b15680.
20. Gao J, Lei H, Han Z, Shi Q, Chen Y, Jiang Y. *Lei H, Han Z, Shi Q, Chen Y, Jiang Y.* Dopamine functionalized tannic-acid-templated mesoporous silica nanoparticles as a new sorbent for the efficient removal of Cu2+ from aqueous solution. Sci Rep. 2017;7(1):45215. https://doi.org/10.1038/srep45215.
21. Lascu A, Palade A, Fagadar-Cosma G, Creanga I, Ianasi C, Sebarchievici I, Birdeanu M, Fagadar-Cosma E. Mesoporous manganese–porphyrin–silica hybrid nanomaterial sensitive to H2O2 fluorescent detection. Mater Res Bull. 2016;74:325–332. https://doi.org/10.1016/j.materresbull.2015.10.032.
22. Dong R, Bo Y, Tong G, Zhou Y, Zhu X, Lu Y. Self-assembly and optical properties of a porphyrin-based amphiphile. Nanoscale. 2014;6(9):4544–4550. https://doi.org/10.1039/C4NR00212A.
23. Meadows PJ, Dujardin E, Hall SR, Mann S. Template-directed synthesis of silica-coated J-aggregate nanotapes. Chem Commun (Camb). 2005;(29):3688–3690. https://doi.org/10.1039/b502436f.
24. Chen X, Zhao T, Zou J. A novel mimetic peroxidase catalyst by using magnetite-containing silica nanoparticles as carriers. Microchim Acta. 2009;164(1-2):93–99. https://doi.org/10.1007/s00604-008-0038-x.
25. Yang W, Zheng H, Yuan WT, Xu J-G. XU J-G. Silica-hemin composite nanoparticles as new biocatalyst to highly sensitive determination of glucose in human serum. Anal Sci. 2004;20(9):1265–1270. https://doi.org/10.2116/analsci.20.1265.
26. Nath A, Dharmadhikari J, Dharmadhikari A, Mathur D, Mazumdar S. Ultrafast dynamics of hemin aggregates. Phys Chem Chem Phys. 2017;19(39):26862–26869. https://doi.org/10.1039/C7CP04858K.
27. Srinivas V, Rao CM. Time profile of hemin aggregation: an analysis. Biochem Int. 1990;21:849–855.
28. Yousefpour M, Taherian Z. The effects of ageing time on the microstructure and properties of mesoporous silica-hydroxyapatite nanocomposite. Superlattices Microstruct. 2013;54:78–86. https://doi.org/10.1016/j.spmi.2012.11.002.
29. Monnier A, Schüth F, Huo Q, Kumar D, Margolese D, Maxwell RS, Stucky GD, Krishnamurty M, Petroff P, Firouzi A, et al. Cooperative formation of inorganic-organic interfaces in the synthesis of silicate mesostructures. Science. 1993;261(5126):1299–1303. https://doi.org/10.1126/science.261.5126.1299.
30. Thommes M, Kaneko K, Neimark AV, Olivier JP, Rodriguez-Reinoso F, Rouquerol J, Sing KSW. Physisorption of gases, with special reference to the evaluation of surface area and pore size distribution (IUPAC Technical Report). Pure Appl Chem. 2015;87(9-10):1051–1069. https://doi.org/10.1515/pac-2014-1117.
31. Kruk M, Jaroniec M, Sakamoto Y, Terasaki O, Ryoo R, Ko CH. Determination of pore size and pore wall structure of MCM-41 by using nitrogen adsorption, transmission electron microscopy, and X-ray diffraction. J Phys Chem B. 2000;104(2):292–301. https://doi.org/10.1021/jp992718a.
32. Sing KSW. Reporting physisorption data for gas/solid systems with special reference to the determination of surface area and porosity (Recommendations 1984). Pure Appl Chem. 1985;57(4):603–619. https://doi.org/10.1351/pac198557040603.
33. Lin HP, Wong ST, Mou CY, Tang CY. Extensive void defects in mesoporous aluminosilicate MCM-41. J Phys Chem B. 2000;104(38):8967–8975. https://doi.org/10.1021/jp001569p.